International Journal of Control and Automation
Vol. 8, No. 1 (2015), pp. 111-124
http://dx.doi.org/10.14257/ijca.2015.8.1.10

A Multiscale Finite Element Model for Avascular Tumor Growth

Changyu Liu [1, 4], Bin Lu [2, *] and Cong Li [3]

[1]*School of Computer Science and Engineering, South China University of Technology, Guangzhou 510006, China*
[2]*School of Computer Science, Wuyi University, Jiangmen 529020, China*
[3]*College of Computer Science, Sichuan Normal University, Chengdu 610068, China*
[4]*School of Computer Science, Carnegie Mellon University, Pittsburgh, PA 15213, USA*
yezhich@gmail.com, [*]lbscut@gmail.com (corresponding author), jkxy_lc@sicnu.edu.cn

Abstract

There are many mathematical models or chemical models available to describe the avascular tumor growth. However, few of them take into account the necessary physical growth for the avascular tumor. In this paper, we proposed a multiscale finite element model that spans three distinct scales for the avascular tumor growth. At the extracellular microenvironment level, we proposed a new set of piecewise reaction diffusion equations to describe the extracellular microenvironment of the tumor growth. At the intracellular cycle level, we proposed a cell cycle control factor to model the key role that played by the G_1-S phase transition. At the cellular level, we introduced the proposed cell cycle control factor to combine the extracellular microenvironment, the intracellular cycle and the cellular cycle into the total energy equations to form our finite element cellular model. Experiments were performed to simulate the growth of EMT6/Ro mouse mammary cell under three different kinds of initial chemical concentrations. Results showed that the proposed approach outperformed the baseline approach in terms of tumor cell number and tumor cell volume.

Keywords: *multiscale, finite element, avascular tumor growth, physical growth*

1. Introduction

It has a profound and far reaching significance to study the prevention and cure of malignant tumors, not only for decreasing the incidence rate and mortality rate, but also for guiding clinical diagnosis and treatment.

During the formation of tumor spheroids, the tumor cells could change their physiology features, genetic transcription process and proteins expression according to the dynamic cellular microenvironment. Due to the fact that the tumor growth is a complex process that involves a cell cycle, a cell interaction and an extracellular microenvironment, the traditional Cellular Potts Model (CPM) [1] and some other extensions of it [3, 5, 7] were too simple to simulate the dynamic microcosmic process of tumor growth and did not combine different scales to understand the internal principles of tumor growth, diffusion and restriction, causing the following limitations: (1) Their models couldn't simulate the evolutionary process for tumor growth from several cells to a huge spheroid. (2) Their models couldn't simulate the cell interaction and the chemical reaction diffusion process on multiple scales. (3) Their models couldn't determine quantitatively the influence of extracellular and intracellular chemicals on tumor growth [9, 11]. (4) The time consumption will become a problem when there are a huge number of cells.

For mathematical modeling of tumor growth, Jiang *et al.* [13] proposed a multi-scale cellular model that consisted of a cellular level, a sub-cellular level and an extracellular level by extending the traditional Cellular Potts Model. Because this approach considered more for the influence from the micro chemical environment than that from the growth

ISSN: 2005-4297 IJCA

dynamic which has something to do with the volume and the surface area of a growing or a quiescent tumor cell, it was not suitable to simulate the tumor growth with an extra larger number of cells.

In order to solve these problems, a multiscale finite element model for avascular tumor growth, which combines an extracellular level, an intracellular level and a cellular level, was proposed in this paper based on the existing Cellular Potts Model [13, 15, 17, 19]. The experimental results demonstrated the effectiveness of our proposed approach.

2. Finite Element Based Multiscale Modeling

2.1. Basic Assumptions

(1) There are three layers from outside to inside of a growth saturated avascular tumor spheroid, which are a proliferating (P) layer, a quiescent (Q) layer and a necrotic (N) layer.

(2) There are three levels, which are an extracellular microenvironment level, an intracellular cycle level and a cellular level for tumor growth modeling.

(3) There is a competition for nutrients among the tumor cells, while there is no such competition among the normal cells and the tumor cells.

2.2. Extracellular Microenvironment Level

At the extracellular microenvironment level, there are mainly two kinds of chemical substances that could influence the tumor growth, which are the nutrients, i.e. oxygen and glucose, and the Growth Inhibitory Factor (GIF). Although chemicals diffuse usually at different rates among proliferating cells, quiescent cells and necrotic cells, we assume, for simplicity, that: (1) the diffusion constants for concentration fields of oxygen, glucose and GIF are three constants, because the cell position related information is already included in the concentration fields of oxygen, glucose and GIF. (2) Each cell is chemically homogeneous and the cell-culture medium outside the spheroid maintains a constant level of metabolites. (3) The diffusion direction for nutrient concentration fields is from the external medium to the internal necrotic zone, while the diffusion direction for the GIF concentration field is opposite. In this paper, we proposed a new set of piecewise reaction diffusion equations to describe the extracellular microenvironment of the tumor growth, as shown in Eq. (1-3), based on paper [21].

$$\frac{\partial N_O(\vec{x},t)}{\partial t} = D_O \nabla^2 N_O(\vec{x},t) - \sigma \alpha_O \sum_{S\in\{P,Q,N\}} \delta_S(\vec{x}) K_O^S N_O(\vec{x},t) \tag{1}$$

$$\frac{\partial N_G(\vec{x},t)}{\partial t} = D_G \nabla^2 N_G(\vec{x},t) - \sigma \alpha_G \sum_{S\in\{P,Q,N\}} \delta_S(\vec{x}) K_G^S N_G(\vec{x},t) \tag{2}$$

$$\begin{aligned}\frac{\partial G(\vec{x},t)}{\partial t} = D_{GIF} \nabla^2 G(\vec{x},t) - \sigma \alpha_{GIF} \sum_{S\in\{P,Q,N\}} \delta_S(\vec{x}) K_{GIF}^S G(\vec{x},t) + \sigma [G_M \\ - G(\vec{x},t)] \sum_{S\in\{O,G\}} \Gamma_S N_S(\vec{x},t)\end{aligned} \tag{3}$$

$$s.t.: \; N_O(\vec{x},0) = N_O^{INT}, N_G(\vec{x},0) = N_G^{INT}, G(\vec{x},0) = G_{GIF}^{INT}, G_M = G_{GIF}^{THR}.$$

where $\vec{x} = (x,y,z)^T$ is a vector for three dimension coordinates, $\left(N_O(\vec{x},t), N_G(\vec{x},t), G(\vec{x},t)\right)$ are the concentration fields vectors of (oxygen, glucose,

GIF), (D_O, D_G, D_{GIF}) are the diffusion constants for the concentration fields of (oxygen, glucose, GIF), $(\alpha_O, \alpha_G, \alpha_{GIF})$ are the control constants for (oxygen, glucose, GIF), σ is the number of tumor cells, $\delta_S(\vec{x}) = 1$ if $\vec{x} \in \Omega_S$, otherwise $\delta_S(\vec{x}) = 0$, and Ω_P, Ω_Q, Ω_N are separately the P layer, the Q layer and the N layer of an avascular tumor spheroid, $\left(K_O^S, K_G^S, K_{GIF}^S \middle| S \in \{P, Q, N\}\right)$ are the consumption or degradation rates of (oxygen, glucose, GIF), $(\Gamma_S | S \in \{O, G\})$ is the saturation rate vector of GIF, $(N_O^{INT}, N_G^{INT}, G_{GIF}^{INT})$ are the initial concentrations of (oxygen, glucose, GIF), and $G_M = G_{GIF}^{THR}$ is the saturation value of GIF.

2.3. Intracellular Cycle Level

At the intracellular cycle level, there are one resting phase G_0 for quiescent cells and four growth phases [24] during a cell cycle, which are the First Growth Phrase (G_1), the Synthesis Phase (S), the Second Growth Phase (G_2) and the Mitotic Phase (M). During the G_1 phase, if the required proteins and growth are unaccomplished, the cell enters G_0 phase, otherwise it would enter the next S phase of the cell cycle, which was also called a G_1-S phase transition. In this paper, we proposed a cell cycle control factor to model the key role that played by the G_1-S phase transition. The proposed cell cycle control factor is defined in Eq. (4), where $F(\vec{x}, t)$ is a cell cycle control factor of a specific tumor cell, $N(\vec{x}, t) = (N_O, N_G)^T$ is a concentration field vector of oxygen and glucose, $\vec{\delta} = (\delta_O, \delta_G)$ is a constant vector for deciding the influence of oxygen and glucose on the local GIF factor level, $N^{THR} = (N_O^{THR}, N_G^{THR})^T$ is a concentration threshold vector of the nutrients, below which the tumor cellular reproduction is inhibited, σ_0 is a influence constant of cell number on the cell cycle control factor, θ is a shape parameter for sigmoid function, and F^{THR} is a threshold of cell cycle control factor.

$$F(\vec{x}, t) = 1 - exp\{\frac{\vec{\delta}[N(\vec{x}, t) - N^{THR}]}{\theta[2 - exp(-\sigma/\sigma_0)][G(\vec{x}, t) - G_{GIF}^{THR}]}\} \tag{4}$$

with

$$F(\vec{x}, t) = \begin{cases} [F^{THR}, 1], & \text{cell becomes proliferating} \\ [0, F^{THR}), & \text{cell becomes quiescent} \\ (-\infty, 0), & \text{cell becomes necrotic} \end{cases}$$

2.4. Cellular Level

At the cellular level, we introduced the proposed cell cycle control factor to combine the extracellular microenvironment, the intracellular cycle and the cellular cycle into the total energy equations [13] to form our finite element (FEM) cellular model, as shown in Eq. (5).

$$H = \sum_{A=1}^{AN} J_A S_A + \sum_{C=1}^{CN} \gamma (V_C - V_C^*)^2 \qquad \text{and} \qquad V_C^* = [1 + \lambda F(\vec{x}, t)] V_C \tag{5}$$

where AN is the global total mesh surface number, CN is the total cell number, A is the global mesh surface identifier that has value among 1~ AN, C is the cell identifier that has value among 1~ CN, S_A is the current area of mesh surface A, V_C is the current volume of cell C while V_C^* is its target cell volume, $J_A \in \{J_A^{PP}, J_A^{PQ}, J_A^{PN}, J_A^{QQ}, J_A^{QN}, J_A^{NN}\}$ is the adhesive coefficient between mesh surface A and its neighbor, $\gamma \in \{\gamma^P, \gamma^Q, \gamma^N\}$ is the coefficient corresponding to the elasticity of the cell volume of C, $F(\vec{x}, t)$ is a cell cycle control factor of the specific tumor cell and λ is a constant volume amplification factor.

From Eq. (5), we can obtain the total energy change ΔH, as

$$\begin{aligned}\Delta H = \sum_{A=1}^{AN} J_A(S_A + dS_A) \\ + \sum_{C=1}^{CN} \gamma(V_C + dV_C - V_C^*)^2 - \sum_{A=1}^{AN} J_A S_A \\ - \sum_{C=1}^{CN} \gamma(V_C - V_C^*)^2 \\ = \sum_{A=1}^{AN} J_A dS_A + \sum_{C=1}^{CN} \gamma(dV_C)^2 - \sum_{j=1}^{CN} 2\gamma \cdot dV_C \\ \cdot (V_C^* - V_C)\end{aligned} \tag{6}$$

$$s.\,t.:\ dS_A = dS_{AL\_C} = \{u\}_{AL\_C}^T \{F_S\}_{AL\_C} + \{u\}_{AL\_C}^T [K_S]_{AL\_C} \{u\}_{AL\_C},$$

$$dV_C = dV_{AL\_C} = \{u\}_{AL\_C}^T \{F_V\}_{AL\_C} + \{u\}_{AL\_C}^T [K_V]_{AL\_C} \{u\}_{AL\_C}.$$

When a tumor cell grows, the total cellular energy will become smaller and smaller with the increase of cellular surface and cellular volume. It will finally reach a critical point for cell division. The equation at this critical point is

$$\partial(\Delta H)/\partial(\{u\}) = 0 \tag{7}$$

After transposition, simplification and terms combination of Eq. (7), a set of finite element equations of tumor growth can be obtained, as

$$[K]\{u\} = \{F\} \tag{8}$$

$$s.\,t.:\ [K] = \sum_{A=1}^{AN} J_A [K_S]_A + \sum_{C=1}^{CN} \gamma \{F_V\}_C \{F_V\}_C^T - \sum_{C=1}^{CN} 2\gamma (V_C^* - V_C)[K_V]_C,$$

$$\{F\} = \sum_{C=1}^{CN} \gamma (V_C^* - V_C)\{F_V\}_C - (1/2) \sum_{A=1}^{AN} J_A \{F_S\}_A.$$

3. Experiments

3.1. Simulation Process

Figure 1 showed an integration of these three cellular levels of our FEM avascular tumor growth model. In the beginning, there is a parameter initialization step which includes: (1) an initialization of diffusion coefficients, initial concentrations, concentration thresholds, and metabolic rates of nutrients and GIF for their P, Q and N stages. (2) an initialization of a lattice with a single central tumor cell ($\sigma = 1$) that described by FEM node structure, edge structure, element structure and cell structure for a specific initial nodes number, such as 18. (3) let the simulation time control variant t of Monte Carlo steps (MCS) be 0. (4) an initialization of other parameters for our FEM tumor growth model as described in table 1. We considered there are 4 MCS, with each MCS for 3 hours growth, in one major loop that represents a cell cycle where we regard G_1, S, G_2 and M as G_1 and S. Thus, a total cell cycle (also a major loop) took 12 hours.

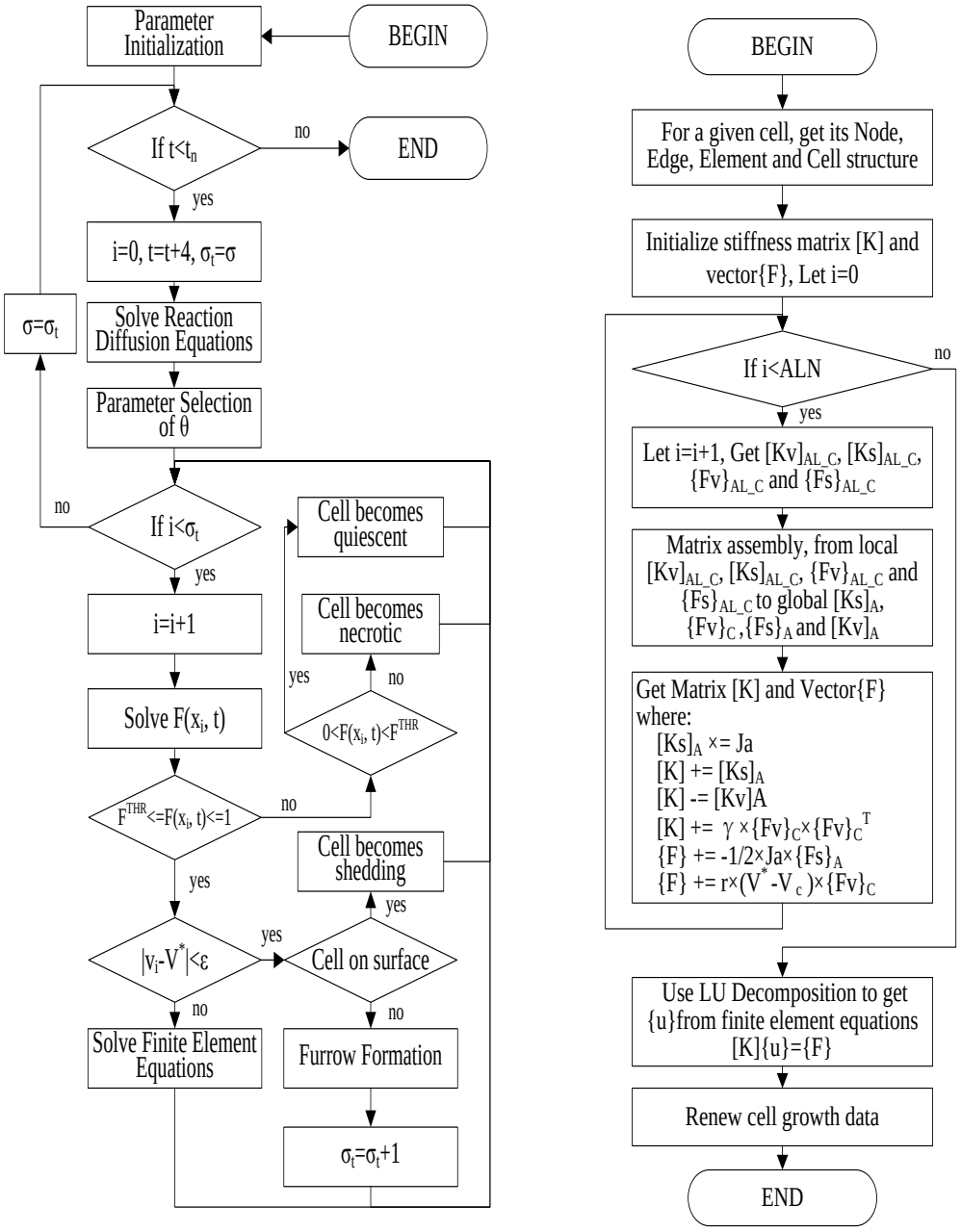

(a) Global Simulation Process (b) FEM Equations Solving Process

Figure 1. Flow Chart for Tumor Spheroid Growth

In Figure 1(a), the G_1 growth phase refers to the initial cell with a specific volume and the first several steps from FEM tumor growth after the G_1-S checkpoint that represented by $F^{THR} \leq F(\overrightarrow{x_i}, t) \leq 1$. The S growth phase refers to several later FEM growth steps that was located between this G_1-S checkpoint and the following cell division. During each iteration, we firstly check if the current simulation time t exceeded the total required time t_n which was set to 40 days (320 simulation steps) in our experiment. If $t < t_n$, the simulation time will proceed one cell cycle $t = t + 4$ that is 12 hours or 4 MCS steps and the current cell number $\sigma_t = \sigma$. The global nutrients concentration $N(\vec{x}, t)$ and GIF concentration $G(\vec{x}, t)$ will be obtained by solving the reaction diffusion equations with a numerical differentiation method in the current time. In order to get the cell cycle control factor $F(\vec{x}, t)$ for each cell, a parameter selection for θ was conducted with a loose search and a fine search. Then, for each cell i in the tumor spheroid that consisted of σ_t cells, we

computed its cell cycle control factor $F(\overrightarrow{x_i}, t)$ with $N(\overrightarrow{x_i}, t)$ and $G(\overrightarrow{x_i}, t)$. After that, we checked the cell cycle control factor value, if: (1) $F(\overrightarrow{x_i}, t) \leq 0$, the current cell will become necrotic. (2) $0 < F(\overrightarrow{x_i}, t) < F^{THR}$, the current cell will become quiescent. (3) $F^{THR} \leq F(\overrightarrow{x_i}, t) \leq 1$, a cell volume check was performed. If the current volume is near to its target volume, the cell will be divided into two daughter cells when it was not on the spheroid surface with a radius more than 0.03 cm, otherwise it will shed from this surface with a 20% probability. If the current volume is much smaller than its target volume, the cell will grow one step by solving a set of finite element equations, as shown in Figure 1(b).

In order to use FEM approach to simulate tumor growth for one step, a Delaunay triangulation was used firstly to get the structure of Node, Edge, Element and Cell and the stiffness matrix $[K]$ as well as the vector $\{F\}$ was initialized. Then, for each mesh surface or element, we: (1) computed its local $[K_V]_{AL\_C}$, $[K_S]_{AL\_C}$, $\{F_V\}_{AL\_C}$ and $\{F_S\}_{AL\_C}$. (2) used the Matrix assembly approach to convert the local $[K_V]_{AL\_C}$, $[K_S]_{AL\_C}$, $\{F_V\}_{AL\_C}$ and $\{F_S\}_{AL\_C}$ to the global $[K_V]_A$, $[K_S]_A$, $\{F_V\}_C$ and $\{F_S\}_A$. (3) got matrix $[K]$ and vector $\{F\}$. (4) used the LU Decomposition to get the growth offset $\{u\}$ from finite element equations $[K]\{u\} = \{F\}$. After this, the model repeats this process until the simulation time expires.

3.2. Simulation Conditions

We used the parameters which were derived from our research partner, the Applied Mathematics and Plasma Physics (T-7) group at Los Alamos National Laboratory, of the mouse mammary tumor cells EMT6/Ro in our experiment. The diffusion coefficients of oxygen, glucose and GIF were derived separately from extensive microelectrode measurements, previous experimental determinations and an iterative process that uses a relative scale to fit the experiment data of growth and inhibitory factors for tumor spheroids [13]. We assume that the nutrients metabolic rates of quiescent cells are half of that for proliferating cells and the metabolic rates of necrotic cells are 0, as shown in Table 1.

Table 1. Model Parameters for EMT6/Ro

Parameters	Oxygen		Glucose		GIF	
	ABBR	Value	ABBR	Value	ABBR	Value
Diffusion Coefficients	D_O	5.94×10^{-2} cm^2/hr	D_G	1.52×10^{-3} cm^2/hr	D_{GIF}	$1.8\times10^{-}3$ cm^2/hr
Initial Concentration	N_O^{INT}	0.08 or 0.28 mM	N_G^{INT}	5.5 or 16.5 mM	G_{GIF}^{INT}	0 mM
Threshold	N_O^{THR}	0.01 mM	N_G^{THR}	0.03 mM	G_{GIF}^{THR}	45 mM
Metabolic Rates (P)	K_O^P	-25 mM/hr	K_G^P	-38 mM/hr	K_{GIF}^P	0 mM/hr
Metabolic Rates (Q)	K_O^Q	-13 mM/hr	K_G^Q	-21 mM/hr	K_{GIF}^Q	50 mM/hr
Metabolic Rates (N)	K_O^N	0 mM/hr	K_G^N	0 mM/hr	K_{GIF}^N	100 mM/hr

Our experiment began with three groups of initial chemical concentrations (N_O^{INT}, N_G^{INT}, G_{GIF}^{INT}), which are: (1) 0.08mM oxygen, 5.5mM glucose, (2) 0.28mM oxygen, 5.5mM glucose, (3) 0.28mM oxygen, 16.5mM glucose, and one initial GIF concentration which was setted to be zero under these three circumstances. Then, we set $\sigma = 1$, $\sigma_0 = 10\text{^}4$, $\vec{\Gamma} = (\Gamma_O, \Gamma_G) = (1,1)$, $\overrightarrow{\alpha_N} = diag(\alpha_O, \alpha_G) = (9 * 10^{-6}, 2 * 10^{-8})$, $\alpha_{GIF} = 8 * 10^{-11}$, $\vec{\delta} = (\delta_O, \delta_G) = (49/50, 1/50)$. Due to the simulation results are not sensitive to the adhesive coefficiency J_A, we use almost the same setting: $J_A^{PP} = J_A^{PQ} = 28$, $J_A^{PN} = 24$, $J_A^{QQ} = J_A^{QN} = 22$, $J_A^{NN} = 0$ for J_A, and $\gamma^P = 1$, $\gamma^Q = 4$, $\gamma^N = 0$ for γ, as in [13]. Besides, parameters of θ and F^{THR} are determined by a set of parameter selection experiments.

3.3. Results for Extracellular Microenvironment Level

The supply of nutrients and the accumulation of GIF in the extracellular microenvironment will influence significantly the cell growth both in in vitro and vivo. The tumor growth simulation began with the solving of a set of reaction diffusion equations. So, it will help understand the growth mechanism of avascular tumor if we know the quantitative knowledge of its surrouding chemical microenvironment. A tumor spheroid will grow from a single cell to a multiscale sturcture with a P layer, a Q layer and a N layer by using the finite element method for the avascular growth. In our experiment, we seek to simulate the relationship between the oxygen concentration, the glucose concentration, the GIF concentration and the tumor growth time which was set to 40 days.

3D Chemical profiles were obtained then on several critical moments. Firstly, the distribution map of oxygen concentration in tumor spheroid that varies with the simulation time and distance from the spehroid core is shown in Figure 2, from a1 to a4. It can be seen that there are several key stages of oxygen concentrations during a tumor growth simulation. In the beginning 0-10.5 days, the oxygen concentration drops all the time and the tumor radius increases rapidly. After 10.5 days growth, a constant area of lower oxygen concentration which is near the threshold is formed in the center of tumor spheroid and the radius of this constant area continues to increase until it reaches its maximum value at 19.5 days growth. Between 19.5 days growth and 30 days growth, the oxygen concentration of this lower area shows a little increase. After 30 days growth, the distribution of oxygen concentration reaches a stable status.

Secondly, the distribution map of glucose is shown in Figure 2, from b1 to b4. It can be seen that the distribution map of glucose is similar with that of oxygen. The only difference between these two nutrients distribution maps lies in the simulation time for such concentration variations. For glucose, 0-13.5 days is its concentration descending period, 13.5-22.5 days is the formation period for its low concentration area, 22.5-31.5 days is a little increase period for the concentration of this lower area and after 31.5 days growth, the distribution of glucose concentration reaches a stable status.

Finally, the distribution map of GIF concentration is shown in Figure 2, from c1 to c4. In contrast with that of nutrients, both the concentration of GIF and the tumor spheroid radius grow with the simulation time. Besides, there is no such lower or higher constant area for GIF concentration. From the distribution maps of oxygen, glucose, and GIF, we can draw the conclusion that the concentrations of oxygen and gulcose from internal tumor spheroid is lower than that from outer tumor spheroid, while the concentration of GIF is on the opposite. Following analysis shows that these resluts were determined by the chemical diffusion coefficients, the width of exhausted area (also N area) and the cell metabolic rate, which would affect the distributions of cell number and cell volume.

3.4. Results for Intracellular Cycle Level

To use the cell cycle control factor $F(\vec{x},t)$ to control the G_1-S transition, we must specify firstly model parameters θ and F^{THR}, which are determined implicitly by specific initial chemical concentrations. In this paper, we performed a two-level parameter selection approach for searching the most suitable parameters θ and F^{THR} in the value space. In order to caculate $N(\vec{x},t)$ and $G(\vec{x},t)$ for $F(\vec{x},t)$, we firstly solved the chemical reaction diffusion equations. Then, we took the center point between the spheroid center and its surface as $\vec{x}$. Last, we took the chemical concentrations at $\vec{x}$ of the tumor spheroid as an input of $N(\vec{x},t)$ and $G(\vec{x},t)$ at the simulation time of 0:30:300 steps.

The final experimental results are $\theta = 0.3$ and $F^{THR} = 0.4381$ for initial concentrations of (oxygen, glucose, GIF) at (0.08 mM, 5.5mM, 0 mM), $\theta = 0.2$ and $F^{THR} = 0.5272$ for these chemicals concentrations at (0.28mM, 5.5mM, 0 mM), $\theta = 0.1$ and $F^{THR} = 0.4656$ for these chemicals concentrations at (0.28mM, 16.5mM, 0 mM).

Once we got the value of θ and F^{THR} through our parameter selection approach, we can then proceed to simulate the whole tumor growth at the cellular level.

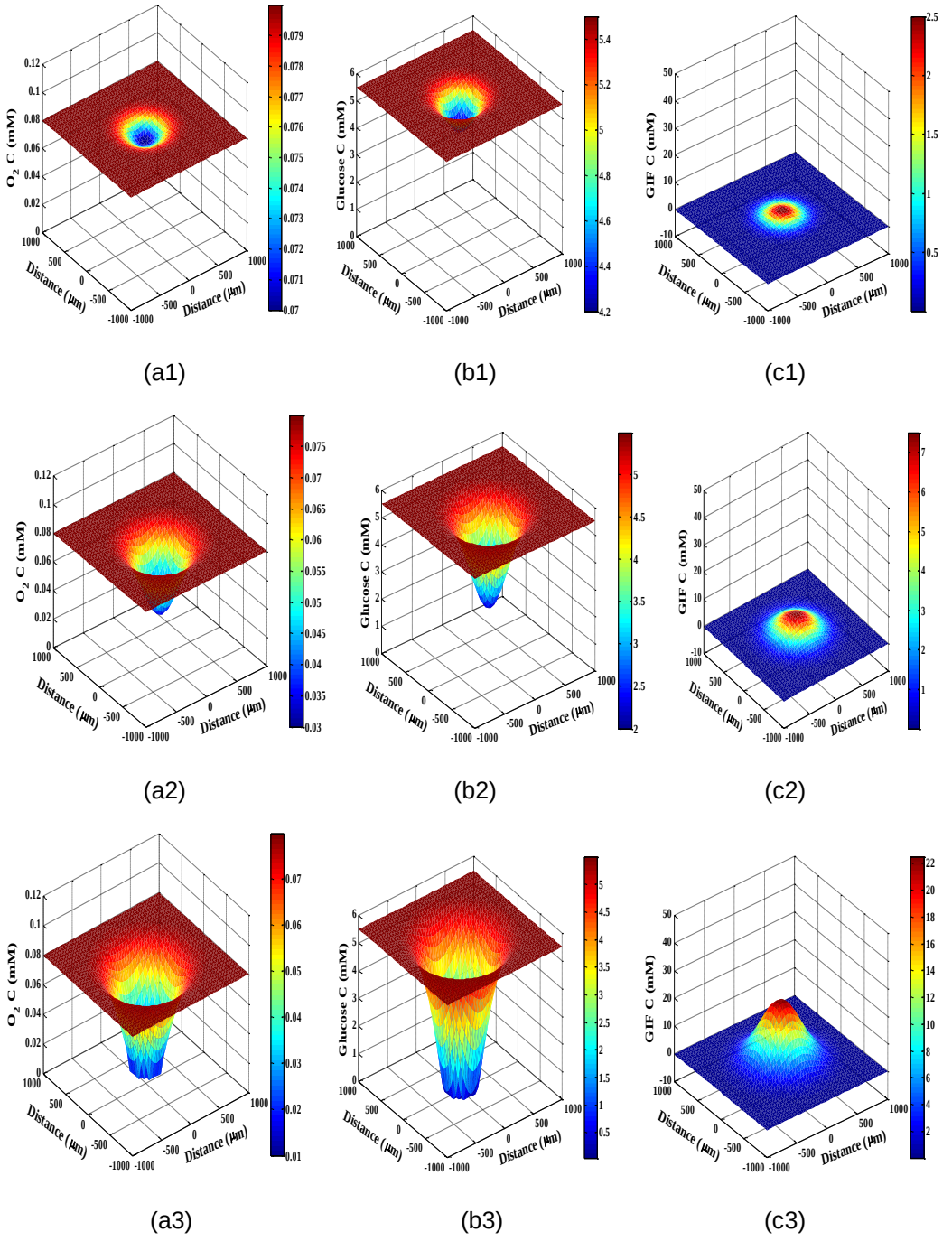

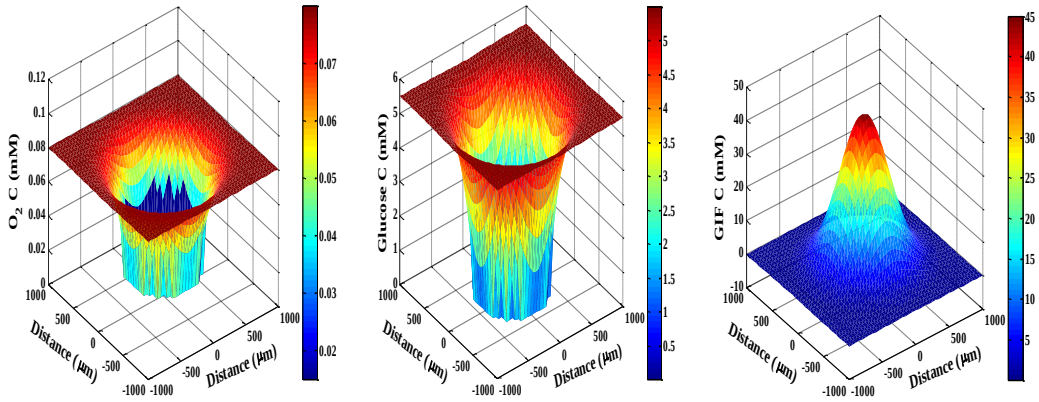

(a4) (b4) (c4)

Figure 2. Chemical Concentration Maps at Sampled Time. (a1-a4) are for Concentration of Oxygen. (b1-b4) are for Concentration of Glucose. (c1-c4) are for Concentration of GIF. The Sampled Days are All 1.5 d, 7.5d, 10.5d and 30d from the Top to the Bottom with an Initial Concentration at (0.08mM Oxygen, 5.5mM Glucose, 0mM GIF)

3.5. Results for Cellular Level

We firstly compared our simulation results with Yijiang's simulation results, and then with the actual data we obtained from our partner T-7 group based on two indexes, which are the cell number and the cell volume. To keep growth balance, a cell shedding rate of 20% was also applied to cells at the surface of tumor spheroid if their radiuses exceed a certain value.

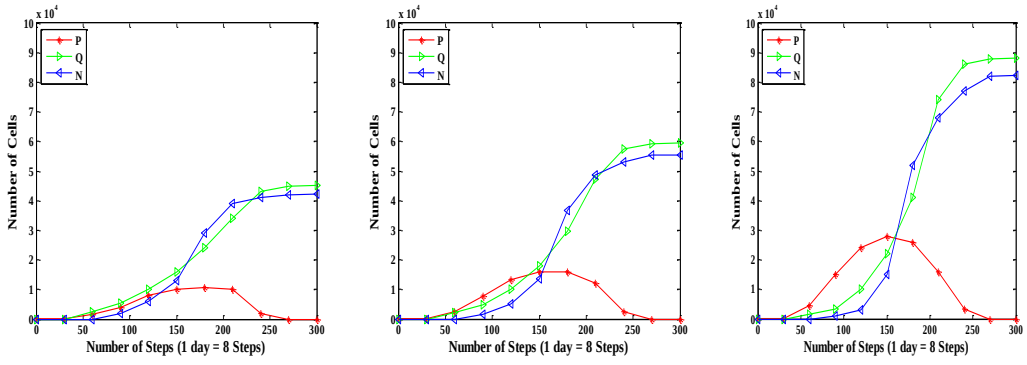

(a1) (a2) (a3)

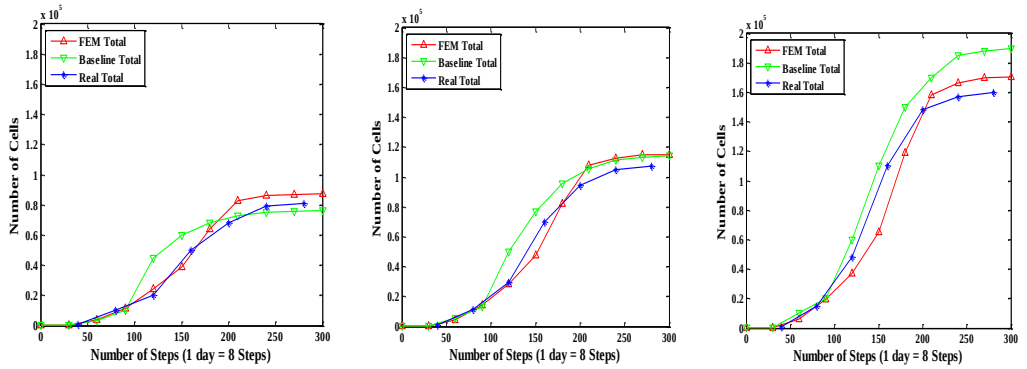

(b1) (b2) (b3)

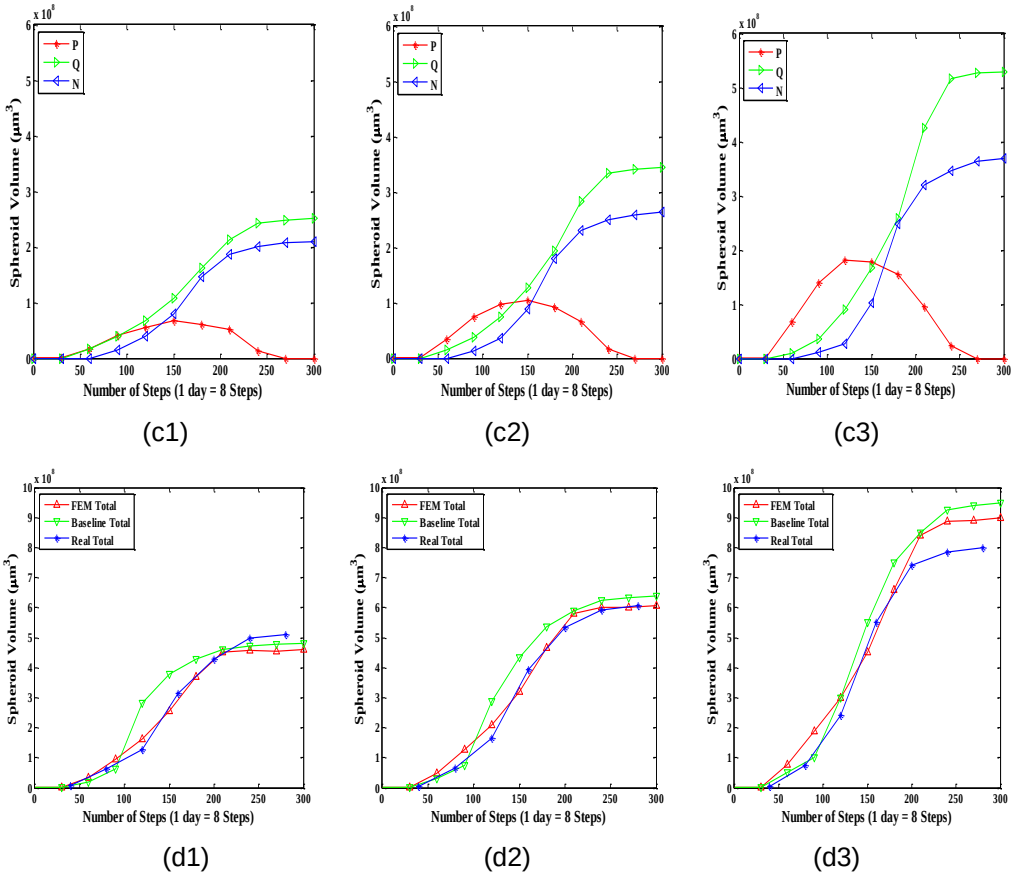

Figure 3. Cell Number and Cell Volume of Tumor Spheroid asFunctions of Simulation Steps. (a1-a3) Show the Cell Number for Layers of P, Q and N. (b1-b3)Show the Total Cell Number for Our FEM Model, the Baseline Model and the Measured Data. (c1-c3) Show the Cell Volume for Layers of P, Q and N. (d1-d3) Show the Total Cell Volume for our FEM Model, the Baseline Model and the Measured Data. (a1, b1, c1, d1) are at Concentration of (0.08 mM Oxygen, 5.5 mM Glucose, 0 mM GIF), (a2, b2, c2, d2) are at Concentration of (0.28 mM oxygen, 5.5 mM glucose, 0 mM GIF), and (a3, b3, c3, d3) are at Concentration of (0.28 mM Oxygen, 16.5 mM Glucose, 0 mM GIF)

Figure 3 (a1) to Figure 3 (b3) show the relationship between the tumor cell number and simulation steps. It can be seen that the tumor cell number reaches an earlier saturation state at 30 days or 240 steps growth, when the division rate equals the shedding rate. Furthermore, the tumor cell number enteres a later saturation state at 40 days or 320 setps growth, following a rapid decrease of proliferating cells. The earlier quiescent cells are generated from cells that don't meet the volume check in the cell cycle. Besides, those quiescent cells would become necrotic when the chemicals concentration drops below the threshold. With an increase of nutrients concentration from (0.08, 5.5), via (0.28, 5.5) to (0.28, 16.5), (1) both the number of PNQ cells and the number of total cells increase accordingly. (2) all kinds of cell numbers increase more rapidly at 0-100 steps than that of 100-300 steps, meaning that there is also an earlier increase on the growth velocity that is caused by a larger concentration of nutrients. (3) the number of P cells grows exponentially in time for 0-150 steps with a following drop due to the appearance of quiescent cells, while that of N cells and Q cells shows a continuous rise for the whole cell cycle. For the total cell number, we compared our data with Yijiang's data and actual

data. The results showed our model is more excellent in simulating a tumor growth under a dynamic chemical environment.

Figure 3 (c1) to Figure 3 (d3) show the relation between the tumor spheroid volume and simulation steps. According to our experiments, the tumor growth also reaches an earlier volume saturation state at 30 days or 240 steps growth. With the increase of tumor cell number, the cell volume also increases, which shows a more or less the same growth trends. However, as we adopted the cell cycle control factor $F(\vec{x}, t)$ for deciding the target cell volume, the size of single tumor cell should: (1) be larger with a higher nutrients concentrations, such as at (0.28mM, 16.5mM) than that (0.08mM, 5.5mM), when other conditions remained unchanged. (2) be larger in P layer than that in Q and N layer due to the nutrients concentrations decreased from the outer medium to the spheroid core. The Figure 3 showed a agreement with these assumptions and our model performed also well in cell volume simulation.

4. Conclusion

In this paper, we proposed a multiscale finite element model for the avascular tumor growth based on three distinct scales, which are an extracellular level, an intracellular level and a cellular level. At the extracellular microenvironment level, we proposed a new set of piecewise reaction diffusion equations to describe the extracellular microenvironment of the tumor growth. At the intracellular cycle level, we proposed a cell cycle control factor to model the key role that played by the G_1-S phase transition. At the cellular level, we introduced the proposed cell cycle control factor to combine the extracellular microenvironment, the intracellular cycle and the cellular cycle into the total energy equations to form our finite element (FEM) cellular model. In the experiments section, we conducted our experiments for the simulation of EMT6/Ro mouse mammary tumor growth. Results showed that the proposed approach outperformed the baseline approach in terms of tumor cell number and tumor cell volume.

Acknowledgments

This paper was supported by the Doctor Startup Foundation of Wuyi University under Grant No. 2014BS07, the Basic Theory and Scientific Research Project of Jiangmen City under title “Research on complex network evolution model and link prediction”, and the National Natural Science Foundation of China under Grant No. 71202165. We would like to thank anonymous reviewers for helpful comments.

References

[1] J. Glazier and F. Graner, “Simulation of the differential adhesion driven rearrangement of biological cells”, Phys. Rev. E., vol. 47, no. 3, **(1993)**, pp. 2128-2154.
[2] C. Y. Liu, “A TPSAC model and its application to mechanical cloud simulation”, Int. J. Secur. Appl., vol. 8, no. 1, **(2014)**, pp. 45-56.
[3] B. M. Rubenstein and L. J. Kaufman, “The role of extracellular matrix in glioma invasion: a cellular Potts model approach”, Biophys. J., vol. 95, no. 12, **(2008)**, pp. 5661-5680.
[4] H. Li, “Catalytic hydrothermal pretreatment of corncob into xylose and furfural via solid acid catalyst”, Bioresource Technol., vol. 158, **(2014)**, pp. 313-320.
[5] J. Adam and N. Bellomo, “A survey of models on tumor immune systems dynamics”, **(1996)**; Birkhäuser, Massachusetts.
[6] J. X. Chen, “Modeling and performance analyzing of helix transmission base on Modelica”, Key Eng. Mater., vol. 455, **(2011)**, pp. 511-515.
[7] J. C. Dallon, “Multiscale modeling of cellular systems in biology”, Curr. Opin. Colloid In., vol. 15, no. 1-2, **(2010)**, pp. 24-31.
[8] C. Liu, “Research on service-oriented and HLA-based simulation model of juice production line”, In ICMTMA, vol. 3, **(2010)**, pp. 167-170.
[9] C. E. Lewis and J. W. Pollard, “Distinct role of macrophages in different tumor microenvironments”, Cancer Res., vol. 66, no. 2, **(2006)**, pp. 605-612.
[10] H. J. Wang, “Structure design and multi-domain modeling for a picking banana manipulator”, Adv.

Mater. Res., vol. 97-101, **(2010)**, pp. 3560-3564.
[11] T. L. Jackson, "Intracellular accumulation and mechanism of action of doxorubicin in a spatio-temporal tumor mode", J. Theor. Biol., vol. 220, no. 2, **(2003)**, pp. 201-213.
[12] H. L. Li, "One-step heterogeneous catalytic process for the dehydration of xylan into furfural", BioResources, vol. 8, no. 3, **(2013)**, pp. 3200-3211.
[13] Y. Jiang, J. P. Grbovic, C. Cantrell and J. P. Freyer, "A multiscale model for avascular tumor growth", Biophys. J., vol. 89, no. 6, **(2005)**, pp. 3884-3894.
[14] C. Y. Liu, "Study on adaptive and fuzzy weighted image fusion based on wavelet transform in trinocular vision of picking robot", J. Inf. Comput. Sci., vol. 11, no. 6, **(2014)**, pp. 1929-1937.
[15] M. Scianna and L. Preziosi, "Multiscale developments of the cellular Potts model", Multiscale Model, Sim., vol. 10, no. 2, **(2012)**, pp. 342-382.
[16] H. Wang, "Study on behavior simulation for picking manipulator in virtual environment based on binocular stereo vision", In ICSC, **(2008)**, pp. 27-31.
[17] A. V. Bohme, "Multi-scale modeling in morphogenesis: a critical analysis of the cellular Potts model", PLOS ONE., vol. 7, no. 9, **(2012)**, pp. 1-14.
[18] H. Li, "A modified biphasic system for the dehydration of D-xylose into furfural using $SO_4^{2-}/TiO^{2-}ZrO_2/La^{3+}$ as a solid catalyst", Catalysis Today, vol. 234, **(2014)**, pp. 251-256.
[19] A. Nakajima and S. Ishihara, "Kinetics of the cellular Potts model revisited", New J. Phys., vol. 13, **(2011)**, pp. 1-9.
[20] B. Lu, "Discovery of community structure in complex networks based on resistance distance and center nodes", J. Comput. Inf. Syst., vol. 8, no. 23, **(2012)**, pp. 9807-9814.
[21] S. C. Ferreira, J. M. L. Martins and M. J. Vilela, "Reaction-diffusion model for the growth of avascular tumor", Phys. Rev. E., vol. 65, no. 2, **(2002)**, pp. 1907-1–1907-8.
[22] Y. Zhang, Y. Zhang, Z. He and X. Tang, "Multiscale fusion of wavelet-domain hidden Markov tree through graph cut", Image Vision Comput., vol. 27, no. 9, **(2009)**, pp. 1402-1410.
[23] C. Liu, "Modeling physical and chemical growths of avascular tumor", Int. J. Multimed. Ubiq. Eng., vol. 9, no. 4, **(2014)**, pp. 349-362.
[24] G. M. Cooper, "The cell: a molecular approach (2nd edition)", Washington, D.C: ASM Press, **(2000)**, pp. Chapter 14.
[25] H. J. Wang, "Study on a location method for bio-objects in virtual environment based on neural network and fuzzy reasoning", In ICIRA, vol. 5928, **(2009)**, pp. 1004-1012.
[26] Y. Zhang, Z. He, Y. Zhang and X. Wu, "Global optimization of wavelet-domain hidden Markov tree for image segmentation", Pattern Recogn., vol. 44, no. 12, **(2011)**, pp. 2811-2818.
[27] A. Hawkins-Daarud, K. G. van der Zee and J. Tinsley Oden, "Numerical simulation of a thermodynamically consistent four-species tumor growth model", Int. J. Numer. Meth. Bio., vol. 28, no. 1, **(2012)**, pp. 3-24.

Authors

Changyu Liu, joined the Communication and Computer Network Lab of Guangdong as a PhD student in 2010 at South China University of Technology, advised by Prof. Shoubin Dong. Then, he joined the School of Computer Science at Carnegie Mellon University as a Visiting Scholar in September 2012 to work with his advisor Dr. Alex Hauptmann. His research interests include machine learning and computer vision.

Bin Lu is currently a lecturer in the School of Computer Science at Wuyi University. He received his Ph.D. degree in 2013 from South China University of Technology. He is a reviewer of the Journal of Yangtze River Scientific Research Institute since 2010. His main research interests include complex network and machine learning.

Cong Li received the PhD degree in Management Science and Engineering from Hefei University of Technology in 2009. He is an associate professor at the College of Computer Science, Sichuan Normal University. His research interests include E-commerce and business intelligence. He is a member of the ACM, and also is a senior member of the China Computer Federation.